Determination and finite element validation of the WYPIWYG strain energy of superficial fascia from experimental data

Marcos Latorre

Escuela Técnica Superior de Ingeniería Aeronáutica y del Espacio
Universidad Politécnica de Madrid
Plaza Cardenal Cisneros, 3, 28040-Madrid, Spain

Estefanía Peña

Aragón Institute of Engineering Research (I3A). Mechanical Engineering Department
University of Zaragoza, Zaragoza, Spain
CIBER de Bioingeniera, Biomateriales y Nanomedicina (CIBER-BBN). Zaragoza. Spain

Francisco J. Montáns*

Escuela Técnica Superior de Ingeniería Aeronáutica y del Espacio
Universidad Politécnica de Madrid
Plaza Cardenal Cisneros, 3, 28040-Madrid, Spain

Abstract

What-You-Prescribe-Is-What-You-Get (WYPIWYG) procedures are a novel and general phenomenological approach to modelling the behavior of soft materials, applicable to biological tissues in particular. For the hyperelastic case, these procedures solve numerically the nonlinear elastic material determination problem. In this paper we show that they can be applied to determine the stored energy density of superficial fascia. In contrast to the usual approach, in such determination no user-prescribed material parameters and no optimization algorithms are employed. The strain energy densities are computed solving the equilibrium equations of the set of experiments. For the case of superficial fascia it is shown that the mechanical behavior derived from such strain energies is capable of reproduc-

*Corresponding author
Email addresses: m.latorre.ferrus@upm.es (Marcos Latorre), fany@unizar.es (Estefanía Peña), fco.montans@upm.es (Francisco J. Montáns)

ing simultaneously the measured load-displacement curves of three experiments to a high accuracy.

Keywords: Biological tissues; orthotropy; hyperelasticity; WYPIWYG hyperelasticity.

1. Introduction

The determination of the mechanical properties of soft tissues is fundamental to better understand the mechanisms that regulate the tissue behavior. A deep knowledge of the mechanical behavior of soft tissue is often the previous step to the determination and fitting of the most appropriate constitutive models to capture the tissue behavior. These constitutive models can be used to feed both mathematical and numerical methods that try to simulate the processes that take place in the human body.

Fascia is a multilayered collagenous tissue found throughout the body that is intimately connected with muscles. The fascia consists of the superficial fascia and the deep fascia. The deep fascia is a dense connective tissue that lies beneath the superficial fascia. Deep fascia is closely linked with a multitude of orthopaedic diseases [1]. The mechanical properties of fasciae strongly affect muscular actions and the development of pathologies, such as acute and chronic compartment syndromes. However, very few studies regarding fascia mechanical properties are available and these are mainly focused on the study of the properties of deep fascia [2, 3] but not on the properties of superficial fascia [4].

The usual approach to modeling the behavior of soft materials under elastic, path-independent (i.e. hyperelastic, non-dissipative) behavior is to propose a form of the stored energy [5]. In the case of anisotropic biological tissues, it is frequent to additionally separate the energy of the ground matrix (including for example elastin) from that of the fibers (collagen) [6]. Since fibers are statistically distributed in the specimen, it is also frequent to propose a distribution function, which can be integrated either fiber-by-fiber in Angular Integration models (AI) [7, 8, 9] or somehow averaged in Generalized Structure Tensor (GST) approaches [9, 10, 11]. Other approaches include homogeneization methods or explicit structural finite element modelling of the constituents [12, 13].

Whereas a purely phenomenological approach has obvious limitations in order to study the theoretical influence of different fiber contents, waviness, linking and distributions in the overall behavior of the composite, the advantage of this approach is that the material is treated as a whole, so there is no need to account for

those fiber distributions, fibre undulations, tension-compression switches [14, 15] or interactions between fibers themselves and between fibers and matrix. Hence, the phenomenological, continuum approach is appealing for modelling biological tissues [5], specially if finite element simulations of organs are to be performed.

What-You-Prescribe-Is-What-You-Get (WYPIWYG) constitutive models for soft materials are purely phenomenological, continuum-based models, in which the material is treated as a whole. Although interpretations in terms of fibers and matrix are also possible, they are not essential in the computational procedure. The basis for these models is WYPIWYG hyperelasticity [16, 17, 18]. WYPIWYG formulations are being employed to model the hyperelastic behavior of soft biological tissues like arteries and skin (Latorre et al, Romero et al, under review). The underlying hypotheses are similar to those employed in infinitesimal elasticity and the number of curves needed to properly define the material are the same as the number of material constants of an equivalent infinitesimal model. If experimental results for a test are not available, engineering judgement may be used to prescribe some values without affecting the predictive capability for the other tests. The salient feature of WYPIWYG formulations is that, once a specific decomposition of the strain energy function is assumed, no analytical shapes of the terms are ever proposed, no user-prescribed material parameters are needed. Thus no optimization procedures are employed to obtain such parameters. Instead, a complete set of experiments that properly define the material behavior is proposed. The equilibrium and compatibility equations of those experiments are numerically solved (up to machine precision if desired) in order to fully determine the WYPIWYG stored energy density of the material at hand. Then, the material behavior may be predicted in any loading situation and in any boundary value problem that may be simulated using, for example, finite elements.

In this paper we apply the WYPIWYG procedure to analyse superficial fascia. We consider this tissue to be a locally transverse isotropic material. The purpose is to show that WYPIWYG procedures are useful for accurately modelling soft biological tissues using a continuum approach which is efficient for finite element analysis. Thus this is an important step towards accurate simulations of surgery in soft tissues.

2. Materials and methods

2.1. Experimental setting and measurements

Superficial fascia were dissected from the hindlimbs of an adult sheep, sacrificed for other study that did not interfere with this work obtained from the slaughterhouse immediately after animal slaughter. After tissue harvesting, the sample

was cleaned by removing excess connective tissue and kept frozen at -18^oC until testing. After thawing, samples were preserved in ion-free PSS (0.9% NaCl) at 4^oC until the preparation of testing samples was carried out. The experimental part was performed by the ICTS "NANBIOSIS" specifically by the Tissue & Scaffold Characterization Unit (U13), of the CIBER in Bioengineering, Biomaterials & Nanomedicine at the University of Zaragoza.

Two dog-bone shaped specimens and one rectangular specimen were punched out of the fascia of the sheep hindlimb by the use of a die cutter with pre-shaped dies of dimensions 30×5 mm and 35×20 mm for uniaxial and simple shear tests, respectively. The thickness of each sample was measured at different locations and then averaged, resulting in $0.392\,\mathrm{mm}$ for the longitudinal uniaxial specimen, $0.257\,\mathrm{mm}$ for the transverse uniaxial specimen and $0.58\,\mathrm{mm}$ for the simple shear specimen. For the uniaxial tests, the die was aligned with its long side either along to or perpendicular to the optically observable collagen fibers in order to obtain the respective longitudinal and transverse specimens [4]. Following a similar setting than that used in [19], the simple shear specimen was mounted in a set of custom clamps on a material testing machine with the fiber direction oriented vertically (parallel to the clamps) with dimensions between clamps of $15.4 \times 15.4\,\mathrm{mm}^2$. The simple tension tests of the dog bones strips and simple shear tests of the fascia strips were performed in a high precision drive Instron Microtester 5548 system adapted for biological specimens. An ultrasonic humidifier was used to avoid specimen drying enabling humidity to be maintained during the test. The displacements map (not needed in the analysis below) and the lengths between the two markers in each direction were measured by a Digital Image Correlation (DIC) Strain Master LaVision System equipped with two high performance digital cameras with a megapixel sensor ($2.5\ [\mu m] \pm 0.5\%$). The tested specimens and the predominant direction $\boldsymbol{a}_3$ of the collagen fibers are shown in Figure 1. The DIC measurements were used to reproduce the initial geometry for the finite element simulations shown below.

Each dog-bone shaped and rectangular shaped sample was preconditioned with four cycles at a nominal strain of 10% based on the measured width of each specimen. The applied displacement rate was $5\,\mathrm{mm}\,/\,\mathrm{min}$ in order to preserve quasi-static testing conditions. The clamp reaction force and global applied displacement from the loading portion of the 4th cycle were used for the material characterization described below.

WYPIWYG procedures need a complete set of experimental data that fully determines the material behavior from a physical standpoint. Given the experimental data available [4], the WYPIWYG procedure for transversely isotropic ma-

terials [17] seems a reasonable assumption for the material at hand. Indeed, this symmetry group needs two complete, tension-compression experimental uniaxial curves (one in the longitudinal, stiffer direction and one in the transverse direction within the isotropic plane) and also one shear test in a plane including the anisotropy direction. The experimental load-displacement curves for both the longitudinal and transverse uniaxial specimens are shown in Figure 2a and 2b—black lines; finite element results will be addressed below. Since uniaxial compression data are not available, the uniaxial stress-strain behavior will be assumed symmetric in tension and compression in terms of Cauchy stresses and logarithmic strains, as we explain below. The experimental load-displacement curve obtained from an additional simple shear test performed over the same material is shown in Figure 2c—again, black lines. The initial horizontal part of this curve, due to the settlement of the experiment before effective loading takes place, has been eliminated. This set of three experimental curves (including the assumed compression branches) uniquely and completely define our material model.

2.2. Constitutive modelling

The WYPIWYG stored energy for incompressible transversely isotropic materials has the following uncoupled form of the deviatoric energy function which is parallel to that of the infinitesimal case but written in terms of logarithmic strains and non-linear dependencies

$$\mathcal{W}\left(\boldsymbol{E}, \boldsymbol{a}_3 \otimes \boldsymbol{a}_3\right) = \omega_{11}\left(E_{11}\right) + \omega_{11}\left(E_{22}\right) + \omega_{33}\left(E_{33}\right) + 2\omega_{13}(E^{\#}_{13}) \tag{1}$$

where $\boldsymbol{E}$ is the isochoric logarithmic strain tensor, $\boldsymbol{a}_3$ is the material preferred direction (usually, the stiffer one), $E_{33} = \boldsymbol{a}_3 \cdot \boldsymbol{E}\boldsymbol{a}_3$ is the logarithmic strain tensor component in that direction, $E_{11} = \boldsymbol{a}_1 \cdot \boldsymbol{E}\boldsymbol{a}_1$ and $E_{22} = \boldsymbol{a}_2 \cdot \boldsymbol{E}\boldsymbol{a}_2$ are in-plane principal logarithmic strains in the isotropic plane $\{\boldsymbol{a}_1, \boldsymbol{a}_2\}$ (i.e. such that $E_{12} = \boldsymbol{a}_1 \cdot \boldsymbol{E}\boldsymbol{a}_2 = 0$) and $E^{\#}_{13} = \sqrt{E^2_{13} + E^2_{23}} > 0$ is the logarithmic shear composite invariant in a plane containing the preferred direction. The functions ω_{ij} and others alike below are the piecewise spline functions to be determined numerically during the computational procedure. In order to guarantee the material-symmetries congruency [20], the stored energy may be computed in practice as the addition of an isotropic (ground matrix) contribution and a tranversely isotropic deviation, i.e.

$$\mathcal{W}\left(\boldsymbol{E}, \boldsymbol{a}_3 \otimes \boldsymbol{a}_3\right) = \mathcal{W}_{iso}\left(\boldsymbol{E}\right) + \mathcal{W}_{tr}\left(\boldsymbol{E}, \boldsymbol{a}_3 \otimes \boldsymbol{a}_3\right) \tag{2}$$

where $\mathcal{W}_{iso}\left(\boldsymbol{E}\right) = \omega\left(E_1\right) + \omega\left(E_2\right) + \omega\left(E_3\right)$ follows the Valanis–Landel decomposition in terms of the (Lagrangian) principal logarithmic isochoric strains E_i, with

$i = 1, 2, 3$, and $\mathcal{W}_{tr}\left(\boldsymbol{E}, \boldsymbol{a}_3 \otimes \boldsymbol{a}_3\right)$ is the anisotropic deviation which follows an analogous decomposition to Eq. (1). For example, during uniaxial tests in which the test axes $\boldsymbol{e}_i$ are coincident with the material preferred axes $\boldsymbol{a}_i$—note that in these cases $E_{ii} \equiv E_i$

$$\begin{aligned}\mathcal{W}\left(\boldsymbol{E}, \boldsymbol{a}_3 \otimes \boldsymbol{a}_3\right) &= \omega_{11}\left(E_{11}\right) + \omega_{11}\left(E_{22}\right) + \omega_{33}\left(E_{33}\right) \\ &= \left[\omega\left(E_1\right) + \tilde{\omega}_{11}\left(E_1\right)\right] + \left[\omega\left(E_2\right) + \tilde{\omega}_{11}\left(E_2\right)\right] + \left[\omega\left(E_3\right) + \tilde{\omega}_{33}\left(E_3\right)\right]\end{aligned} \tag{3}$$

where the axial deviation from the isotropic response is given in these specific cases by the terms $\omega_{ii}^{tr} \equiv \tilde{\omega}_{ii}$. On the other hand, during a pure shear test in the plane $\{\boldsymbol{e}_1, \boldsymbol{e}_3\}$, with $\boldsymbol{a}_3 = 1/\sqrt{2}\left(\boldsymbol{e}_1 + \boldsymbol{e}_3\right)$, the principal Cauchy stress in the test direction $\boldsymbol{e}_1$ is—note that in this case $E_{13}^{\#} \equiv E_{13} = E_1 > 0$ [17]

$$\sigma_1\left(E_1\right) = \omega_{13}'\left(E_1\right) = \omega'\left(E_1\right) + \tilde{\omega}_{13}'\left(E_1\right) \tag{4}$$

and the shear deviation from the isotropic response is given in this specific case by the term $\omega_{13}^{tr} \equiv \tilde{\omega}_{13}$.

If we explicitly consider a ground matrix contribution, the first derivative functions to be determined through the WYPIWYG procedure are ω', $\tilde{\omega}_{11}'$, $\tilde{\omega}_{33}'$ and $\tilde{\omega}_{13}'$. These functions are piece-wise spline functions, i.e. cubic polynomials. The number of pieces is given by the desired accuracy. The determination of the (total) axial terms $\omega_{11}'\left(E\right) = \omega'\left(E\right) + \tilde{\omega}_{11}'\left(E\right)$ and $\omega_{33}'\left(E\right) = \omega'\left(E\right) + \tilde{\omega}_{33}'\left(E\right)$ is performed solving numerically the system of (coupled) equations resulting from both tension-compression uniaxial tests in directions 1 and 3, following the procedure presented in [17] which we enhance below. If the compression parts of the uniaxial test curves are not available, an assumption must be made. These branches are needed in order to compute the stored energy, but they do not affect the results of the corresponding tensile branches (i.e. the extension parts of the uniaxial test curves). The shear (deviation) function $\tilde{\omega}_{13}(E_{13}^{\#})$ may be determined from different tests, as for example a pure shear test just factoring out $\tilde{\omega}_{13}'\left(E_1\right)$ from Eq. (4). Other possibilities are a simple shear test [17], see below as well, or a non-coaxial uniaxial tensile test, but in these two cases it is required the previous knowledge of the axial functions. Further details on the procedure for the determination of these functions are given in [17] and [20].

3. Results

3.1. Simple tension tests

In order to compute the stress-strain uniaxial responses shown in Figure 3, we have initially assumed equivalent rectangular uniaxial specimens with homogeneous stress fields, i.e. ideal uniaxial specimens. Minimum cross-sectional area of each specimen are considered in order to compute the stresses from the measured load at the grips (ordinates in Figure 2). This gives a reference cross-sectional area of $2.40 \times 0.392\,\mathrm{mm}^2$ for the longitudinal strip and a reference cross-sectional area of $2.45 \times 0.257\,\mathrm{mm}^2$ for the transverse strip. Following the analysis and recommendation given in Ref. [21], we also considered an effective length of 95% of the actual distance between grips in order to compute the strains from measured displacements between grips (abscissae in Figure 2). This gives a reference effective length of $15.39\,\mathrm{mm}$ for the longitudinal specimen and a reference effective length of $12.16\,\mathrm{mm}$ for the transverse specimen. The results of these computations are the stress plots shown with cross $(\times)$ lines in Figure 3a. Subsequently, these stress-strain curves have been slightly smoothed to eliminate experimental noise (specially present in the transverse specimen, Fig. 2b). The result of this smoothing operation is shown as continuous lines in Figure 3a.

From these continuous stress-strain curves we can compute the first derivative functions of the terms present in Eq. (3), i.e. ω', $\tilde{\omega}'_{11}$ and $\tilde{\omega}'_{33}$. The computed derivative functions of the stored energy (total) axial terms are shown in Figure 3b. We note that WYPIWYG procedures are computational ones, so the reader should not expect an analytical expression of the stored energy function. Then, no material parameters to modulate such expression are needed. The result of the computational procedure are piecewise polynomials (tens or even hundreds of cubic polynomials depending on the desired accuracy; we typically use 10 to 50) which are visually summarized in the plots of Figure 3b. These strain energy derivatives may be employed to solve numerically any problem, using for example MATLAB for the case of homogeneous deformations or using a finite element program for the case of non-homogeneous deformations. The stress plots shown in Figure 3a as red circles have been computed using MATLAB from these stored energy functions assuming homogeneous tensile tests. With WYPIWYG procedures, the predictions that we *get* from the *prescribed* experimental stress-strain data set are *exact* to any desired, computationally possible, precision. It can be seen in Figure 3a that predicted and prescribed curves are coincident. The reason is that we have numerically solved the boundary value problem of the experiments without imposing the shape of the stored energy terms in Eq. (3).

During the computation of the stored energy axial terms ω'_{11} and ω'_{33}, the non-linear relation between transverse and axial strains (by Poisson's effect) for the test about the isotropic direction 1 is computed as a byproduct. In Figure 3c we show the solution transverse-to-axial relation $E_2^{(1)}(E_1)$ for the uniaxial test in the isotropic direction, hence the superscript (1). In this plot we show as dashed red lines the ranges for the allowed domain for the search of the solution. The upper limit $E_2^{(1)}(E_1) = -\frac{1}{3}E_1$, i.e. $\nu_{12} = \frac{1}{3}$ and $\nu_{13} = 1 - \nu_{12} = \frac{2}{3}$, corresponds to an applicability boundary of the Inversion Formula for the test in direction 3 (see [17]) and the lower limit $E_2^{(1)}(E_1) = -E_1$, i.e. $\nu_{12} = 1$ and $\nu_{13} = 0$, to another boundary with the meaning of a positive Poisson effect ($\nu_{13} > 0$) which is to be expected in most materials, including biological tissues, and which some material models used in biomechanics fail to predict [22]. Even in the case that the solution were out of these reasonable bounds, an alternative Inversion Formula is possible. In Figure 3c we also show the linear extrapolation from the infinitesimal behavior.

With the computed axial terms ω', $\tilde{\omega}'_{11}$ and $\tilde{\omega}'_{33}$ given in Figure 3b, present in the general decomposition of Eq. (2), respective finite element simulations of the longitudinal and transverse tensile tests over the actual specimens have been performed. These simulations have been performed using the commercial general-purpose finite element program ADINA, where the WYPIWYG procedures have been included via a material user subroutine. In Figure 4 we show the undeformed original meshes, the deformed meshes and the von Mises effective stress maps. The elements used are fully integrated $8-$node trilinear finite elements with mixed $u - p$ formulation to avoid volumetric mesh locking (there is no appreciable shear locking in this type of test).

It is seen in Figure 4 that even though the actual geometries of the specimens are not specially close the to ideal ones, the stress distributions are rather uniform along the loading path. This explains in part the excellent results shown in Figures 2a and 2b. In Figures 2a and 2b the red lines with circles are the computed load-displacement curves obtained from the finite element simulations using the meshes given in Figure 4. Each circle corresponds to one step out of the ten steps used in total in the finite element simulation, which was performed using an implicit plain Newton-Raphson algorithm for equilibrium iterations. It can be concluded that the first assumption of ideal uniaxial geometry is adequate for this type of tests in biological tissues. Indeed, we note that in these simulations we have used the shear term $\tilde{\omega}'_{13}$ obtained in the next section, also present in the general decomposition of Eq. (2) and required by the material user subroutine, but it has proven to be somehow irrelevant when obtaining the global load-displacement curves of Figure 2, which reinforces the premise of ideal uniaxial geometry again

and the absence of shear locking.

3.2. Simple shear test

Following the setting given in [19], similar to that given in [23] and [24] for simple shearing, a square specimen was considered for the simple shear test, see Image (c) in Figure 1. As in [19] (see also [26] for a similar case) we considered this test to represent an ideal simple shear test; i.e. a test with a homogeneous stress field. To compute the stress-strain shear curve shown in Figure 5, we have initially considered a cross-sectional area for shearing of $L \times t = 15.4 \times 0.58\,\mathrm{mm}^2$ in order to compute the stresses from the measured vertical load at the grips (ordinates in Figure 2c). The amount of shear strain, from which the logarithmic tensor shear component E_{13} is defined [17], is obtained from the measured displacement at grips (abscissae in Figure 2c) as $\gamma_{13} = u/d$, with $d = 15.4\,\mathrm{mm}$. The results of these operations (and the associated smooth continuous curve) are shown in Figure 5a.

From this continuous stress-strain curve we can compute the first derivative function of the anisotropic shear term present in Eq. (4), i.e. $\tilde{\omega}'_{13}$. Since the available stress-strain curve is that of a simple shear case, we compute the function $\tilde{\omega}'_{13}$ using Eq. (85) of Ref. [17], where we have to use the already known functions $\tilde{\omega}'_{11}$ and $\tilde{\omega}'_{33}$ and the simple shear (deviation) stresses $\tilde{\sigma}_{13} = \sigma_{13} - \sigma^{iso}_{13}$, where σ_{13} are the total shear stresses of Figure 5a and σ^{iso}_{13} are the simple shear stresses derived from the isotropic function $\omega^{iso}(E) \equiv \omega(E)$. The stress plots shown in Figure 5a as red circles have been computed using MATLAB from the stored energy function (note that in this case all the terms are involved) assuming a homogeneous simple shear test. Again, the predictions *gotten* for the *prescribed* experimental stress-strain data set are *exact* (up to machine precision).

In a finite element setting, this ideal test may be simulated using a single trilinear element. In this case the finite element predicts homogeneous stresses and an exact solution of the represented ideal test (the one in an infinitesimal element). In Figure 5b we show the load-displacement predictions for the ideal test against the experimental data if we consider the latter to be an ideal simple shear test, i.e. using a 8-node trilinear $Q1/P0$ element. With the WYPIWYG approach one *gets* the *prescribed* behavior and it is seen that the ideal load-displacement behavior is also captured.

However as it is well-known [27], the actual experimental setting is not an ideal simple shear one mainly because of the length-to-width ratio of the specimen. Then, the stresses are not homogeneous within the specimen and the problem is a general boundary value problem which is to be solved using finite elements; the approach also followed in [19]. To this end we employed a fine mesh of fully

integrated $Q2/P1$ elements which are optimal mixed quadratic elements with a linear pressure field and known to pass the inf-sup condition. As it can be seen in Figure 6a the stress distribution is not homogeneous. It is well-known, and it can be observed in the figure, that in this case the free surfaces have a shape similar to a cubic polynomial, an effect that is weaker in soft biological tissues because of the low shear stiffness of the ground matrix. Then, the shown shear stress distribution is far from being constant at the grips, reaching a maximum at the corners of the specimen. As a consequence, the predictions of a mesh that accurately reproduces the boundary value problem of the experiment are not in accordance with experimental data because in order to obtain the stored energy employed in such simulations we have considered that the load-displacement curve was obtained from an ideal simple shear experiment, which was not the case. In Fig. 5b we show that using just a single $Q2/P1$ element, the predicted load-displacement curve differs substantially from the ideal one but it is in fact very close to the respective actual solution using a fine mesh of Q2/P1 elements (c.f. Fig. 6b). We here emphasize that proper finite elements are to be used to model biological tissues in general and the simple shear test in particular in order to avoid the well-known issues of volumetric and shear locking which affect the standard formulation; and also to avoid hourglass modes specially present in same elements when large stiffness ratios are expected, as it is the case of biological tissues.

In the WYPIWYG approach, the non-homogeneous finite element solution of the actual test simulation may be used to compute the correct ideal simple shear load-displacement and stress-strain curves. We explain next a very simple iterative procedure that gives both the correct ideal (homogeneous) solution and the corresponding correct actual (nonhomogeneous experimental) solution.

Let k denote the iteration counter. In order to obtain the *ideal* stress-strain curve $\sigma_{13}^{(0)}(E_{13})$ of Figure 5a in the iteration *zero* ($k = 0$), we have considered $F_{ideal}^{(0)} = F_{exp}$, where F_{exp} is the measured *experimental* load of Figure 2c and $F_{ideal}^{(k)} = \sigma_{13}^{(k)} A_{exp}$ is the resultant load of an ideal test where $\sigma_{13}^{(k)}$ is the ideal, uniform stress. Then we obtained the associated shear stresses as $\sigma_{13}^{(0)} = F_{ideal}^{(0)}/A_{exp}$, with A_{exp} being the actual specimen cross-sectional area for shearing, i.e. $A_{exp} = L \times t = 15.4 \times 0.58\,\mathrm{mm}^2$. This allowed us to compute the strain energy shear term function $\tilde{\omega}_{13}^{\prime(0)}(E_{13}^{\#})$. Subsequently, a proper finite element simulation of the actual simple shear test setting (see Figure 6a) using the function $\tilde{\omega}_{13}^{\prime(0)}(E_{13}^{\#})$ gave the *actual* FEM-computed vertical load $F_{actual}^{(0)}$, see Figure 6b, just by integration of the shear stress distribution in the clamps —in practice the sum of the reactions in the

shearing direction at each clamp

$$F^{(k)}_{actual}\left(u\right) = \int_{A_{exp}} \sigma^{(k)}_{13}\left(u\right) dA \tag{5}$$

Clearly, $F^{(0)}_{actual} < F_{exp}$, which means that the primary assumption $F^{(0)}_{ideal} = F_{exp}$ was not correct. We propose the following iterative procedure for $F^{(k)}_{ideal}$, which converges to the solution F_{ideal} in very few iterations—just take $\alpha^{(0)} = 1$ in order to initialize the procedure

$$\begin{cases} \text{1. } F^{(k)}_{ideal} = \alpha^{(k)} F_{exp} \rightarrow \sigma^{(k)}_{13} = \dfrac{F^{(k)}_{ideal}}{A_{exp}} \overset{\text{WYPIWYG}}{\longrightarrow} \tilde{\omega}'^{(k)}_{13} \overset{\text{FEM, Eq. (5)}}{\longrightarrow} F^{(k)}_{actual} \\ \text{2. If } \quad \left| F^{(k)}_{actual} - F_{exp} \right| < tol \quad \Rightarrow \quad F_{ideal} = F^{(k)}_{ideal} \text{ (converged, exit)} \\ \qquad \text{otherwise update } \alpha^{(k+1)} = \alpha^{(k)} \dfrac{F_{exp}}{F^{(k)}_{actual}} \text{ and go to Step 1} \end{cases} \tag{6}$$

This iterative process converged to $\alpha^{(4)} = 1.75$ in just four iterations. In Figure 6b we show the results obtained from the respective boundary value problem with nonhomogeneous solution during each considered iteration. For $k = 4$ the load-displacement predictions are very close to the measured experimental values. Interestingly, we note that

$$\sigma^{(k)}_{13} = \frac{F^{(k)}_{ideal}}{A_{exp}} = \frac{\alpha^{(k)} F_{exp}}{A_{exp}} = \frac{F_{exp}}{A_{exp}/\alpha^{(k)}} = \frac{F_{exp}}{A^{(k)}_{ideal}} \tag{7}$$

so one can consider that the ideal loading curve is being corrected (increased) through $F^{(k)}_{ideal} = \alpha^{(k)} F_{exp}$ preserving the value of the cross-sectional area A_{exp} or, equivalently, that the (effective) cross-sectional area of the ideal simple shear test is being corrected (decreased) through $A^{(k)}_{ideal} = A_{exp}/\alpha^{(k)}$ preserving the value of the experimental loading F_{exp}.

Obviously the correct material characterization must be performed with the corrected load-displacement curve whose derived stress-strain curve simulates an ideal, homogeneous simple shear test, i.e. that given by $F_{ideal} = F^{(4)}_{ideal} = \alpha^{(4)} F_{exp} = 1.75 \times F_{exp}$. We show in Figure 7a the converged stress-strain curve obtained from $F^{(4)}_{ideal}$ and A_{exp} and the derived strain energy shear term in Figure 7b. Remarkably, because the strains in fascia are only moderately large, the stored

energy derivative term ω'_{13} has values close to those of σ_{13}. However, for very large strains both curves become very different in general.

The proper correction for the experimental loading curve is given in Figure 7c. In this figure we show the original experimental curve, the corrected one, finite element simulations using specimens with more adequate aspect ratios to represent the ideal simple shear test, and a finite element simulation of the actual experiment (square specimen) using an adequate finite element mesh. It is seen that, again, the behavior is correctly predicted for both the ideal homogeneous simple shear case (simulated by $L/d = 10$ in the figure) and the actual nonhomogeneous experimental setting ($L/d = 1$ in the figure). We note that the iterative procedure was performed only for the value of the maximum displacement in the experiment. However, remarkably we have captured the behavior at all displacement levels even though the problem is obviously nonlinear—we also show the final results in Figure 2c for the reader convenience.

The herein described iterative procedure is much simpler and intuitive than the one given in [19] (also similar to many other works) for the material characterization using simple shear tests with square-shaped specimens and typical hyperelastic models. However we note that, when possible, specimens with large aspect ratios should be employed in this test to avoid this iterative procedure and the need of solving a nonhomogeneous problem via finite element analysis as to obtain the behavior of the solid under these more general conditions (note that all the results with $L/d = 10$ are almost coincident in Figure 7c). We note that square or cube-shaped specimens are used to test different biological tissues, see for example [23, 24, 25]. However, the stress state within these specimens are far from homogeneous [27], a fact that should be taken into consideration when fitting material parameters from experimental data obtained this way (recall that we obtained $\alpha = F_{ideal}/F_{exp} = 1.75$). To this end, as we have herein shown, a finite element analysis of the experiment using the constitutive model being calibrated allows to perform this correction in an iterative manner.

4. Discussion

In modelling soft biological tissues several approaches have been proposed. Probably structure-based approaches are currently favoured in the literature. In these approaches a distinction between the contribution of the collagen fibres and the rest of the components (elastin, and nonfibrous molecules) is considered. There are different proposals of this kind in the literature (each one with its own merits and inconveniences) as angular integration (AI) of statistical distributions of collagen fibres (e.g. [7, 8]), General Structure Tensor approaches (GST)

(e.g. [10, 11]), multiscale approaches (e.g. [13, 28]) and non-affine models (e.g. [29, 30]). The last ones emphasize the fact that the stress and strain fields are different for the components and then contradict the assumption made in affine models. It is interesting to note that despite of the micromechanical motivation and structure of these models, the constitutive equations for the components are usually phenomenological (for example Fung-type for fibers and Neokookean for matrix) and the paramaters of these constitutive models are typically obtained from a fit of the measured experimental behavior on the composite as a whole [6, 11, 31, 32], frequently even using inverse analysis over *continuum* finite element structures [31, 32]; although recently more efforts are placed on using the specific histological data to obtain at least some material parameters. The structure-based approach would suggest to employ just parameters from experimental data of the components and from histological data, avoiding phenomenological, macroscopic fitting of any microstructural material parameter, specially when multiple solutions are possible and frequently reported, see for example [31, 32, 33]. Furthermore, the computationally efficient General Structure Tensor schemes used in finite element simulations of organs compute *continuum* stresses from *average* (and affine) strains of components in a nonlinear problem, which is another approximation which reduces their accuracy [9]. Just as an example of the difficulties encountered following the GST structure-based approach in a general problem, we note that the formulation may result in an inadequate consideration of the fibers working in tension and those working in compression. Solutions have been proposed just recently within the AI framework in Refs. [14, 34] and within the GST framework in Ref. [15].

Phenomenological continuum models have also been extensively used when modelling biological tissues, see for example [31]. However, the parameters of the proposed stored energies are also typically obtained though optimization procedures. In this work, we also follow the phenomenological continuum approach. Whereas with this approach it is not possible to see the influence of fiber content and distributions in the overall behavior of the composite, the continuum nature of the model is in accordance with the continuum nature of the experiments employed, and the computational efficiency is parallel to that of the usual phenomenological models as Ogden's model (Crespo et al, under review). WYPIWYG approaches have some very appealing characteristics: (1) they are motivated in the infinitesimal theory and, in contrast to many formulations [35] recovers that theory in the limit (preserving also the insight from the infinitesimal framework in the finite strain regime); (2) they use the same decomposition as that of the equivalent infinitesimal framework and do not impose the shape of the associated strain

energy non-linear terms; (3) they do not use user-prescribed material parameters nor optimization procedures; (4) the solution is unique; (5) the prescribed stress-strain curves are exactly captured and (6) the computational efficiency for finite element analysis is similar to that of classical phenomenological models.

WYPIWYG procedures solve the following mathematical problem: Find the *unique* material which following the hypothesis given by Eqs. (1)-(4) behaves *exactly* as measured (or prescribed) in a complete set of experiments. The material behavior will then be exactly captured in any other loading situation and boundary value problem if those hypotheses hold. Regarding this issue we note that the Valanis-Landel decomposition used in the isotropic part is widely accepted and holds mathematically for the moderately large deformations present in biological tissues. The decomposition used for the anisotropic contribution is also the one used in the linear case and similar in nature to the ones used in many other structure-based models, where the energy of the fibers is added to that of the matrix. WYPIWYG procedures may be used to obtain the material behavior from load-displacement curves in nonhomogeneous problems. With the insight from the linear theory, an iterative nonlinear procedure may be established to obtain first the stress-strain curves and then the corresponding WYPIWYG strain energy density terms to apply to other problems. These stored energies may be efficiently used in finite element simulations of organs.

As it can be seen in the final result of Figure 2, we have shown that WYPIWYG procedures are useful for modelling accurately the behavior of soft tissues for finite element analysis in general and for fascia in particular. We show that the computed load-displacement behavior for longitudinal, transverse and simple shear specimens have an exceptional correlation with the experimental measurements. Of special interest is the performed simple shear test because it results in non-homogeneous stress and strain fields. We show that even for this case we are able to capture the load-displacement curve to a high accuracy via finite element analysis of the actual experiment using a simple, physically sound intuitive procedure.

Acknowledgements

Partial financial support for this work has been given by grants DPI2015-69801-R and DPI2013-44391-P from the Dirección General de Proyectos de Investigación of the Ministerio de Economía y Competitividad of Spain. F.J. Montáns also acknowledges the support of the Department of Mechanical and Aerospace Engineering of University of Florida during the sabbatical period in which this paper was finished, and Ministerio de Educación Cultura y Deporte of Spain for the

financial support for that stay under grant PRX15/00065. The ADINA program license used for this work has been a courtesy of ADINA R&D to the Universidad Politécnica de Madrid.

References

[1] Wang, H.Q., Y.Y. Wei YY, T. Sacks, Z. Wu, Z.J. Luo. Impact of leg lengthening on viscoelastic properties of the deep fascia. BMC Musculoskelet. Disord. 10:105–110, 2009.

[2] Eng, C. M., F. Q. Pancheri, D. E. Lieberman, A. S. Biewener, L. Dorfman. Directional Differences in the Biaxial Material Properties of Fascia Lata and the Implications for Fascia Function. Ann. Biomed. Eng. 42:1224–1237, 2014.

[3] Pancheri, F.Q., C. M. Eng, D. E. Lieberman, A. S. Biewene, L. Dorfman. A constitutive description of the anisotropic response of the fascia lata. J. Mech. Behav. Biomed. Mater. 30:306–323, 2014.

[4] Ruiz-Alejos, D., J. A. Peña, M. M. Perez, E. Peña. Experiments and constitutive model for deep and superficial fascia. Digital Image Correlation and finite element validation. Strain, in press. DOI: 10.1111/str.12198, 2016

[5] Humphrey, J.D. Cardiovascular Solid Mechanics: Cells, Tissues, and Organs. Springer, New York, 2013.

[6] Holzapfel, G.A., T. Gasser, R. W. Ogden. A new constitutive framework for arterial wall mechanics and a comparative study of material models. J. Elast. 61:1–18, 2000.

[7] Lanir, Y. A structural theory for the homogeneous biaxial stress-strain relationships in flat collagenous tissues. J. Biomech. 12(6):423–436, 1979.

[8] Lanir, Y. Constitutive equations for fibrous connective tissues. J. Biomech. 16(1):1–12, 1983.

[9] Cortes, D. H., S. P. Lake, J. A. Kadlowec, L. J. Soslowsky, D. M. Elliott (2010). Characterizing the mechanical contribution of fiber angular distribution in connective tissue: comparison of two modeling approaches. Biomech. Model. Mechanobiol. 9(5), 651-658, 2010.

[10] Freed, A. D., D. R. Einstein, I. Vesely. Invariant formulation for dispersed transverse isotropy in aortic heart valves: an efficient means for modeling fiber splay. Biomech. Model. Mechanobiol. 4(2–3):100–117, 2005

[11] Gasser, T., R. Ogden, G. A. Holzapfel. Hyperelastic modelling of arterial layers with distributed collagen fiber orientations. J. R. Soc. Interface, 3:13–35, 2006.

[12] Lake, S.P., M. F. Hadi, V. K. Lai, V. H. Barocas. Mechanics of a fiber network within a non-fibrilar matrix: Model and comparison with collagen.agarose co-gels. Ann. Biomed. Eng. 40(10):2111–2121, 2012.

[13] Zang, L., S. P. Lake, V. K. Lai, C. R. Picu, V. H. Barocas, M. S. Shephard. A coupled fiber-matrix model demonstrates highly inhomogeneous microstructural interactions in soft tussues under tensile load. J. Biomech. Egrg. 135(1):011008, 2013.

[14] Holzapfel, G. A., R. W. Ogden. On the tension-compression switch in soft fibrous solids. Eur. J. Mech. A Solids, 49:561–569, 2015.

[15] Latorre, M., F. J. Montáns. On the tension-compression switch of the Gasser-Ogden-Holzapfel model: Analysis and a new pre-integrated proposal. J. Mech. Behav. Biomed. Mater. 57, 175-189, 2016.

[16] Sussman, T., K. J. Bathe. A model of incompressible isotropic hyperelastic material behavior using spline interpolations of tension-compression test data. Commun. Numer. Methods Eng. 25(1):53–63, 2009.

[17] Latorre, M., F. J. Montáns. Extension of the Sussman–Bathe spline-based hyperelastic model to incompressible transversely isotropic materials. Comput. Struct., 122:13–26, 2013.

[18] Latorre, M., F. J. Montáns. What-You-Prescribe-Is-What-You-Get orthotropic hyperelasticity. Comput. Mech., 53(6): 1279–1298, 2014.

[19] Weiss, J. A., J. C. Gardines, C. Bonifasi-Lista. Ligament material behavior is nonlinear, viscoelastic and rate-independent under shear loading. J. Biomech. 35:943–950, 2002.

[20] Latorre, M., F. J. Montáns. Material-symmetries congruency in transversely isotropic and orthotropic hyperelastic materials. Eur. J. Mech. A Solids 53:99–106. 2015.

[21] Tian, L., J. Henningsen J, M. R. Salick, W. C. Crone, M. Gunderson, S. H. Dailey, N. C. Chesler. Stretch calculated from grip distance accurately approximates mid-specimen stretch in large elastic arteries in uniaxial tensile tests. J. Mech. Behav. Biomed. Mater. 47, 107-113, 2015.

[22] Skacel, P., J. Bursa. Poisson's ratio of arterial wall–Inconsistency of constitutive models with experimental data. J. Mech. Behav. Biomed. Mater. 54, 316-327, 2016.

[23] Dokos, S., B. H. Smaill, A. A. Young, I. J. LeGrice. Shear properties of passive ventricular myocardium. Am. J. Physiol. Heart. Circ. Physiol. 283(6), H2650-H2659, 2002

[24] Sommer, G., M. Eder, L. Kovacs, H. Pathak, L. Bonitz, C. Mueller, P. Regitnig, G. A. Holzapfel. Multiaxial mechanical properties and constitutive modeling of human adipose tissue: A basis for preoperative simulations in plastic and reconstructive surgery. Acta Biomat. 9: 9036–9048, 2013.

[25] Sommer, G., A.J. Schriefl, M. Andra, M. Sacherer, C. Viertler, H. Wolinski, G.A. Holzapfel. Biomechanical properties and microstructure of human ventricular myocardium. Acta Biomat. 24: 172–192, 2015.

[26] Holzapfel, G.A., R. W. Ogden. Constitutive modelling of passive myocardium: a structurally based framework for material characterization. Philos. Trans. R. Soc. Lond. A Math. Phys. Eng. Sci. 367(1902), 3445-3475, 2009.

[27] Horgan, C.O., J. G. Murphy. Simple shearing of soft biological tissues. Proc. R. Soc. Lond. A Math. Phys. Eng. Sci. 467: 760–777, 2011.

[28] Stylianopoulos, T., V. H. Barocas. Multiscale, structure-based modeling for the elastic mechanical behavior of arterial walls. J. Biomech. Engrg. 129(4): 611–618, 2007.

[29] Chandran, P.L., V. H. Barocas. Affine versus non-affine fibril kinematics in collagen networks: theoretical studies of network behavior. J. Biomech. Engrg. 128: 259–270, 2006

[30] Chen, H., Y. Liu, X. Zhao, Y. Lanir, G. S. Kassab. A micromechanics finite-strain constitutive model of fibrous tissue. J. Mech. Phys. Solid 59(9):1823–1837, 2011

[31] Evans, S.L., C. A. Holt. Measuring the mechanical properties of human skin in vivo using digital image correlation and finite element modelling. J. Strain Anal. 44:337–345, 2009.

[32] Groves, R.B., S. A. Coulman, J. C. Birchall, S. L. Evans. An anisotropic, hyperelastic model for skin: Experimental measurements, finite element modelling and identification of parameters for human and mourine skin. J. Mech. Behav. Biomed. Mater. 18:167-180, 2013.

[33] M. Abbasi, M.S. Barakat, K. Vahidkhah, A. N. Azadani. Characterization of three–dimensional anisotropic heart valve tissue mechanical properties using inverse finite element analysis. J. Mech. Behav. Biomed. Mater. in press. DOI: dx.doi.org/10.1016/j.jmbbm.2016.04.031

[34] Li, K., R. W. Ogden, G. A. Holzapfel. Computational method for excluding fibers under compression in modeling soft fibrous solids. Eur. J. Mech. A Solids 57, 178–193, 2016.

[35] Murphy, J.G. Evolution of anisotropy in soft tissue. Proc. R. Soc. Lond. A Math. Phys. Eng. Sci. 470 (2161), 20130548, 2014.

Figures

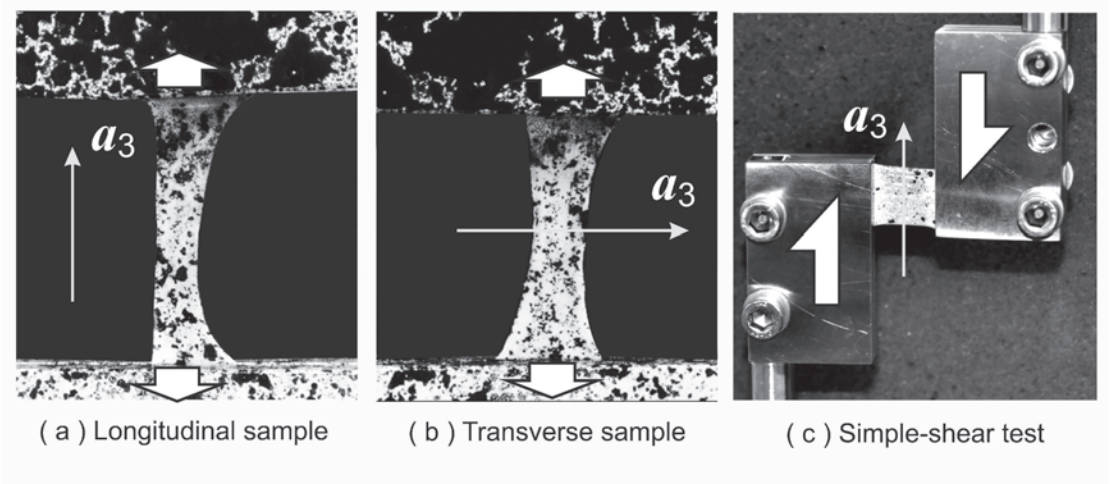

Figure 1: Principal anisotropy direction $\boldsymbol{a}_3$ over images of the specimens mounted in a uniaxial testing device for longitudinal (a) and transverse (b) specimens and in a simple shear device (c)

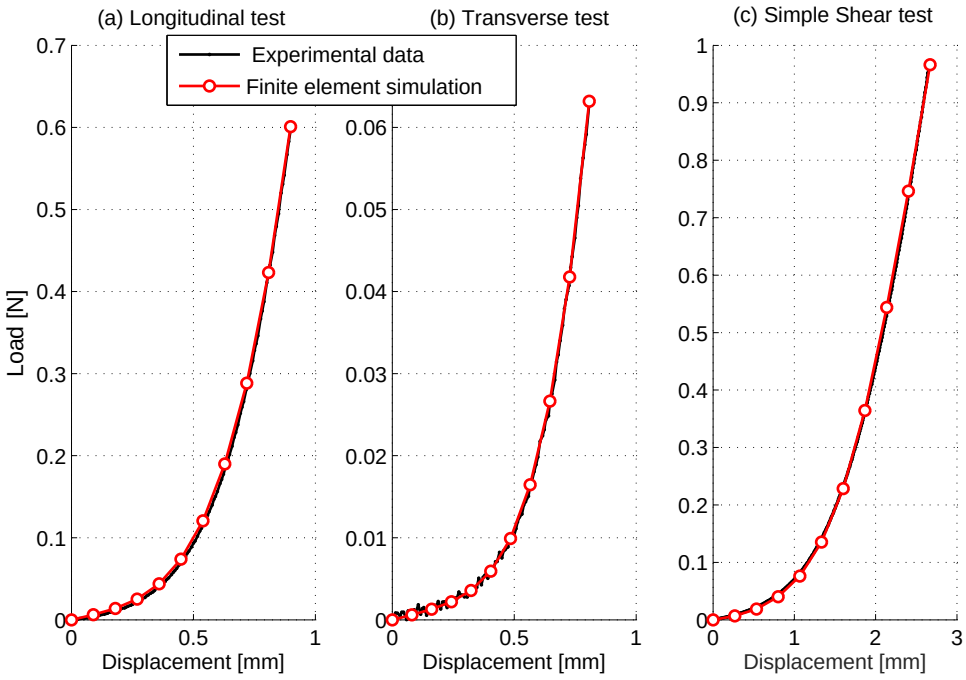

Figure 2: Experimental load-displacement data and finite element computed results for the longitudinal uniaxial specimen (a), the transverse uniaxial specimen (b) and the simple shear specimen (c)

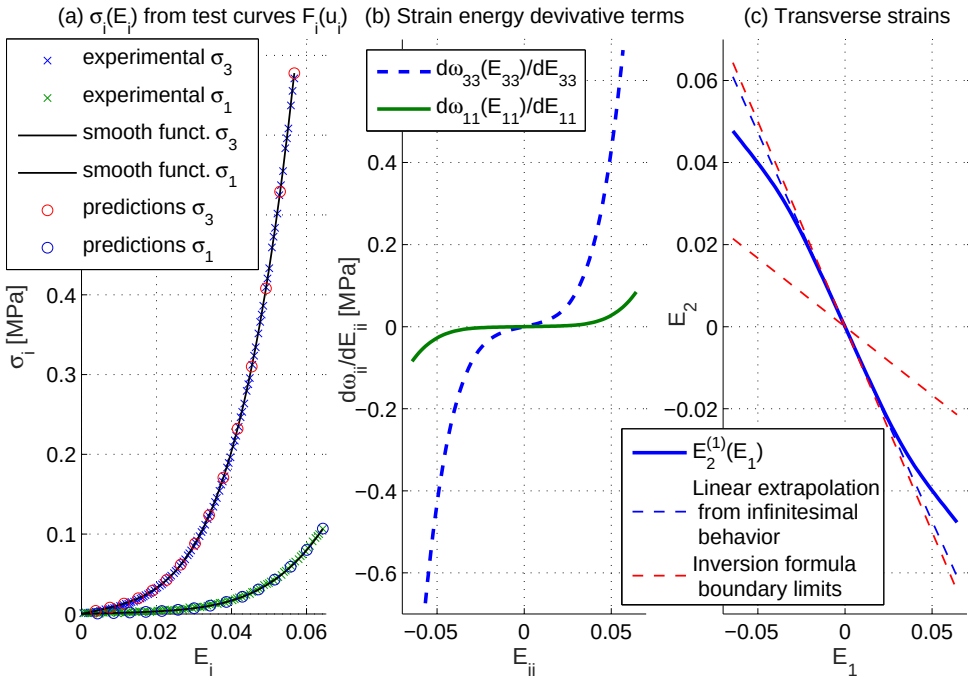

Figure 3: (a) Stress-strain response curves for ideal uniaxial tests. Experimental stresses are those obtained directly from the load-displacement curves shown in Figure 2 using the respective minimum cross-sectional areas and effective distances between grips (95%). Smooth stress plots are slightly smoothed stresses from experimental data as to eliminate experimental noise. Predicted stress plots are the stresses derived from the computed WYPIWYG stored energy function shown in (b). (b) First derivative functions of the (total) axial terms $\omega'_{ii}(E_{ii}) = \omega'(E_{ii}) + \tilde{\omega}'_{ii}(E_{ii})$ of the stored energy density, see Eq. (3). The isotropic contribution $\omega'(E)$, not shown explicitly, has been previously computed assuming an isotropic tension-compression uniaxial response $\sigma(E) = 0.9 \times \sigma_1(E)$, see (a), and the symmetries $\sigma_i(-E_i) = -\sigma_i(E_i)$ have been considered for the uniaxial compression branches. (c) Computed nonlinear transverse strains relation $E_2^{(1)}(E_1)$ for a test performed in direction 1. Red dashed lines are the limits of applicability of the usual inversion formula and of positive Poisson effect (a solution is searched within these limits).

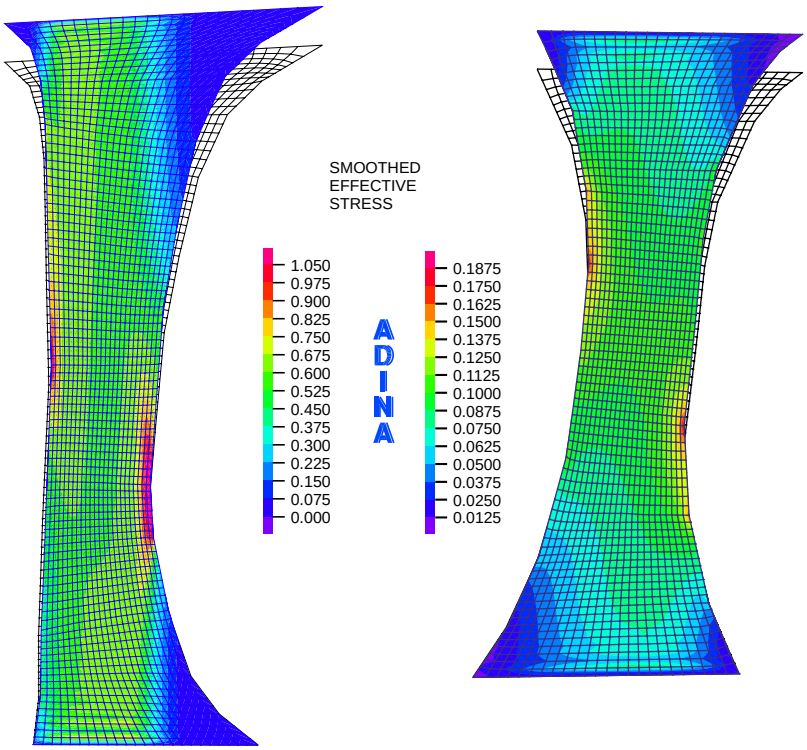

Figure 4: Finite element simulations of longitudinal (left) and transverse (right) actual specimens. Undeformed meshes (in black), deformed meshes and effective von Mises stresses (colormaps over the deformed meshes). Smoothed von Mises (or effective) stresses have been obtained from extrapolation to nodes and nodal averaging

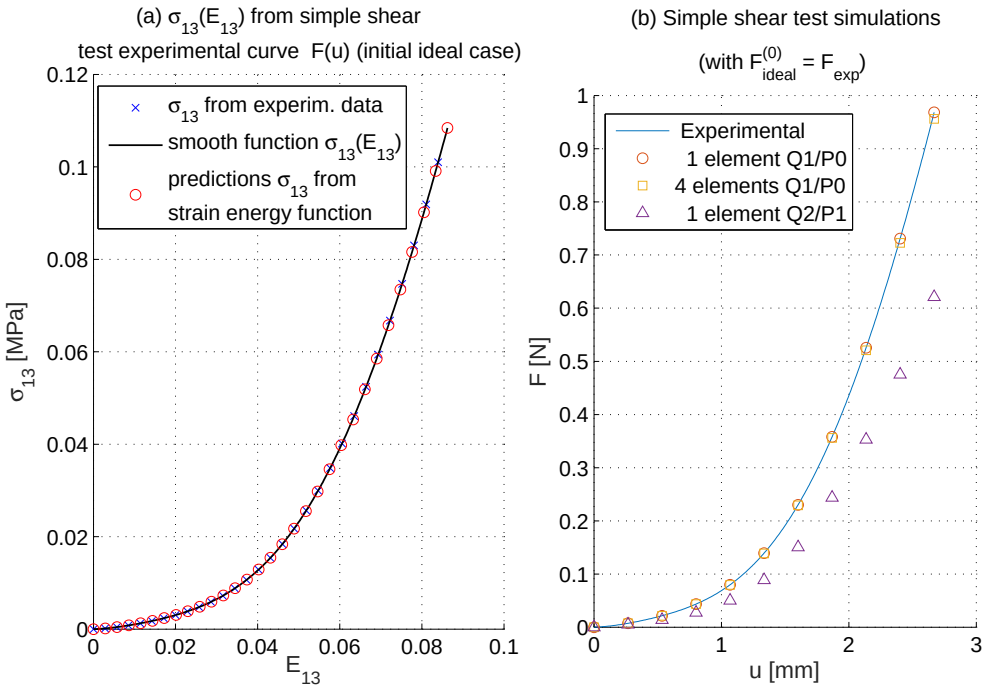

Figure 5: (a) Stress-strain response curve derived from an ideal simple shear test (with $F^{(0)}_{ideal} = F_{exp}$, see below). Experimental stresses are those obtained directly from the load-displacement curve shown in Figure 2c using the actual (i.e. total) cross-sectional area for shearing. Smooth stress plots are slightly smoothed stresses from experimental data as to eliminate experimental noise. Predicted stress plots are the stresses derived from the computed WYPIWYG stored energy function (not shown at this initial stage). (b) Simple shear load-displacement curves treating the experimental load-displacement data as if obtained from an ideal simple shear test ($F^{(0)}_{ideal} = F_{exp}$, see below), i.e. using the strain energy that derives from the stresses depicted in (a). Note that $Q1/P0$ finite elements reproduce the ideal setting, but not the corresponding real one because they lock in shear. The adequate $Q2/P1$ element shows that the experiment is far from an ideal simple shear test and stresses are not uniform inside the specimen.

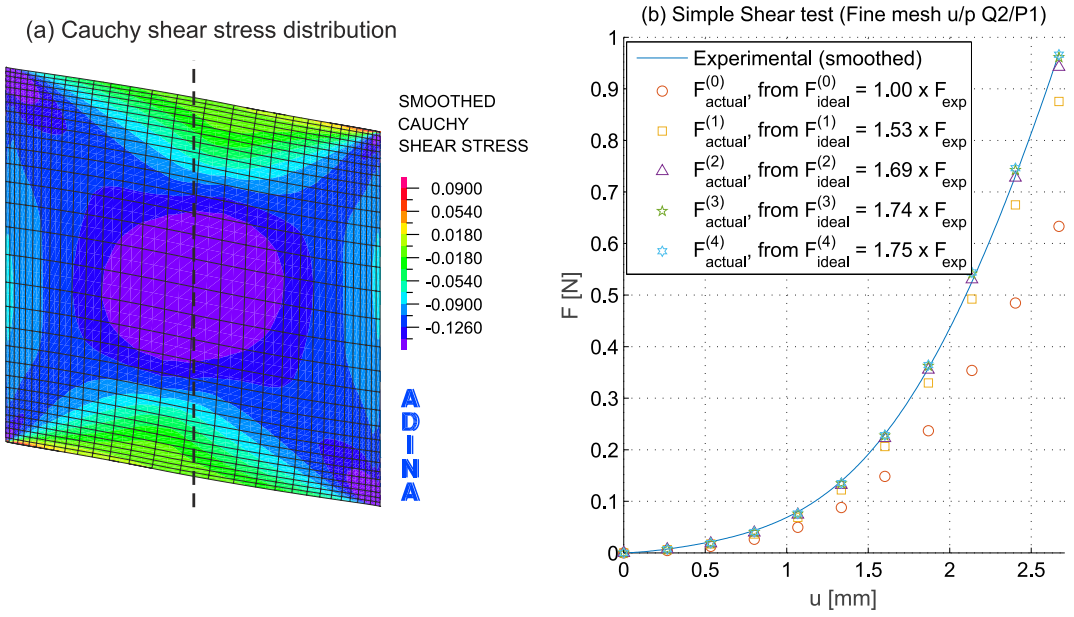

Figure 6: (a) Displacement field and shear stress field in the configuration of the performed experiment. (b) Iterative correction applied to the ideal simple shear loading curve ($F^{(k)}_{ideal} = \alpha^{(k)} F_{exp}$) to recover the actual simple shear test ($F_{actual} \simeq F_{exp}$). The four iterations are shown. It is seen that the converged load-displacement ideal response $F^{(4)}_{ideal} = 1.75 F_{exp}$ (or equivalent effective area $A^{(4)}_{ideal} = 0.57 A_{exp}$) yields a very accurate conversion between the experimental setting and an ideal simple shear test at all strain levels. Note that the value of $A^{(4)}_{ideal} = 0.57 A_{exp}$ could be approximately deduced directly from the stress discribution (a) using a simple engineering reasoning of stress equivalence

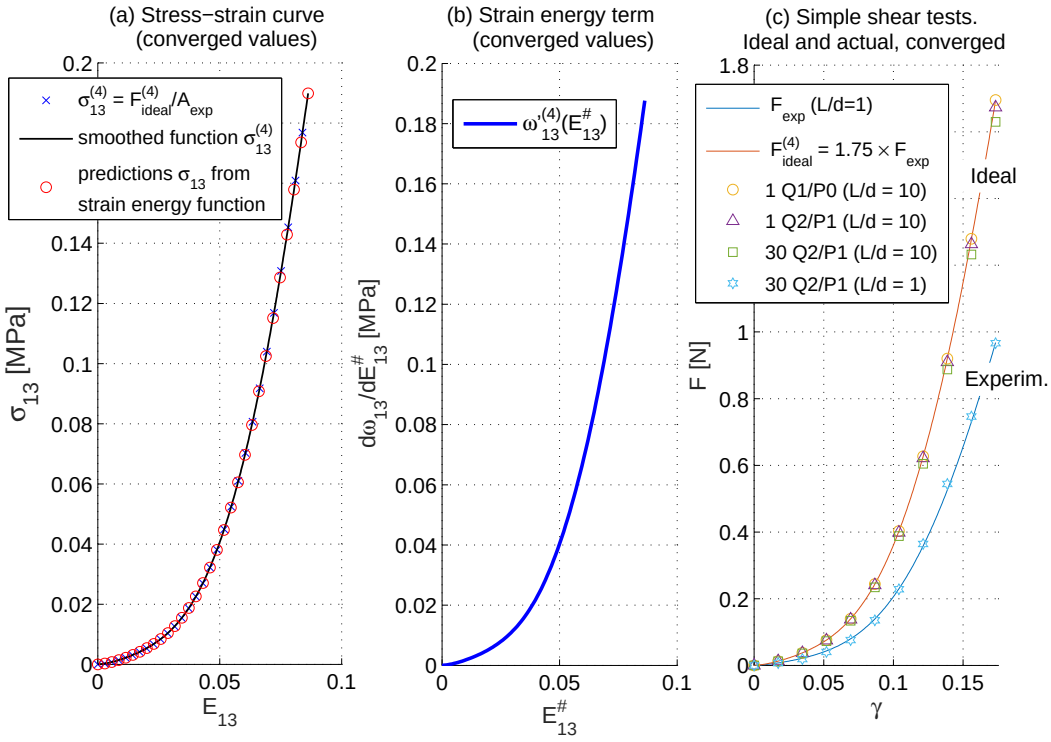

Figure 7: (a) Stress-strain (discrete and smoothed) simple shear responses derived from the proper ideal simple shear test, with $F^{(4)}_{ideal} = 1.75F_{exp}$ (compare to Figure 5a). (b) Corresponding first derivative function of the (total) shear term $\omega'_{13}(E_{13}) = \omega'(E_{13}) + \tilde{\omega}'_{13}(E_{13})$ of the stored energy density, see Eq. (4). The isotropic contribution $\omega'(E)$, not shown explicitly, has been previously computed assuming an isotropic tension-compression uniaxial response $\sigma(E) = 0.9 \times \sigma_1(E)$, see Figure 3. Predicted stresses in (a) are the stresses derived from the complete WYPIWYG stored energy function; i.e. shear term shown in (b) and axial terms shown in Figure 3b. (c) Ideal and actual simple shear loading curves for the square specimen under study. It can be observed that all the shown finite element simulations with aspect ratios of $10 : 1$ (close to an ideal test with homogeneous distributions) tend to the same ideal response and that the simulation with aspect ratio of $1 : 1$ (the experimental layout in this paper, resulting in a nonhomogeneous stress field) reproduces the experimental loads. The results are presented in terms of the amount of shear $\gamma = \gamma_{13}$ in order to make the cases $L/d = 10$ and $L/d = 1$ comparable to each other.